

pubs.acs.org/acsapm Article

Suppressing Water Uptake and Increasing Hydroxide Conductivity in Ring-Opened Polynorbornene Ion-Exchange Materials via Backbone Design

Jamie C. Gaitor, Megan Treichel, Tomasz Kowalewski,* and Kevin J. T. Noonan*



Cite This: ACS Appl. Polym. Mater. 2022, 4, 8032–8042



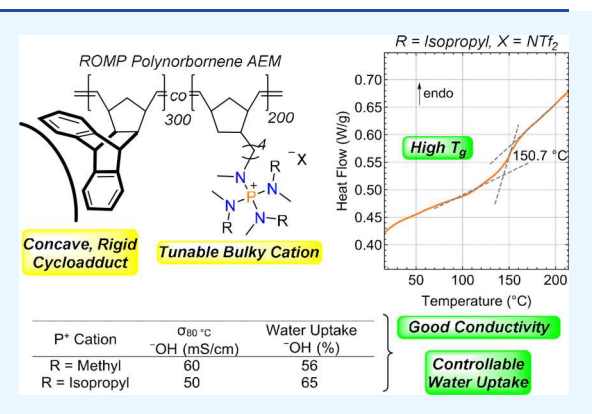
ACCESS I

III Metrics & More

Article Recommendations

Supporting Information

ABSTRACT: In this study, we aimed to decrease segmental mobility in ring-opened polynorbornene anion-exchange membranes (AEMs) as a strategy to suppress swelling. This was accomplished by copolymerization of a norbornene-anthracene cycloadduct with cationic tetraaminophosphonium norbornene monomers to afford AEMs with glass transition temperatures above 100 °C. The anthracenyl side groups appended to the poly(vinylene-1,3-cyclopentylene) chain resulted in lower water uptake for the phosphonium-functionalized AEM when compared to an analogue without the arene moiety. Though chemical aging of these AEMs was noted over time, the benefits of rigidifying the polymer backbone were clear. Additionally, we have noted that the choice of dialkylamino groups around the phosphorus center plays a key role in alkaline stability of these phosphonium-based AEMs.



KEYWORDS: tetraaminophosphonium polymers, trimethylammonium polymers, ring-opened polynorbornenes, statistical copolymers, anion-exchange membranes, alkaline stability

■ INTRODUCTION

In recent years, there has been extensive work on anionexchange membranes (AEMs) to facilitate selective transport of hydroxide anions in electrochemical devices. 1-8 Synthesis of AEMs is typically accomplished by direct polymerization of cationic monomers or by postpolymerization modification of a polymer backbone decorated with reactive groups. Direct polymerization of cationic monomers is particularly useful when the cation itself is difficult to synthesize or when quantitative postpolymerization functionalization is challenging. To this end, ruthenium-catalyzed ring-opening metathesis polymerization (ROMP) is exceptional for direct polymerization of cationic monomers due to the mild reaction conditions required for this reaction (Figure 1A)9 and tolerance to a wide range of different ionic groups. 10-2 However, some of the AEMs prepared using ROMP swell considerably in aqueous environments (water uptakes > 100%), 10-27 which can be detrimental to the mechanical integrity of the material over time. Swelling is related to the type of tethered cation chosen for transport, the ion-exchange capacity (IEC) of the material, and the choice of polymer backbone.

The typical polyolefins prepared using ROMP, such as polynorbornenes and polyalkenamers, have flexible backbones and low glass transition temperatures ($T_{\rm g}$ < 50 °C), ²⁸ which may play a role in the water uptake (WU) observed for ROMP-based AEMs. Several researchers have demonstrated

that chemical crosslinking can reduce swelling in these AEMs, 11,15,22,25,27 which can be partially attributed to the decrease in segmental mobility of the polymer backbone upon crosslinking. Inspired by recent work on high $T_{\rm g}$ cyclic olefin polymers prepared using ROMP, ^{29,30} we demonstrate that copolymerization of a rigid norbornene anthracene cycloadduct with tetraaminophosphonium norbornenes can also be used to decrease segmental mobility in polynorbornene-based AEMs, which results in reduced swelling and improved hydroxide conductivity (σ) when compared to the flexible hPN-co-iPrMe analogue (Figure 1B). The unsaturated PNBAn-co-Phos derivatives had higher conductivities than the saturated ones at 80 °C, providing support that decreasing segmental mobility is beneficial in these phosphonium copolymers. In addition, stability studies in 10 M KOH revealed the importance of bulky isopropyl groups on the amino substituents around the phosphorus atom for improved stability toward hydroxide. Though embrittlement of the PNBAn-co-Phos AEMs was noted over time, the study

Received: February 17, 2022 Accepted: September 8, 2022 Published: October 13, 2022





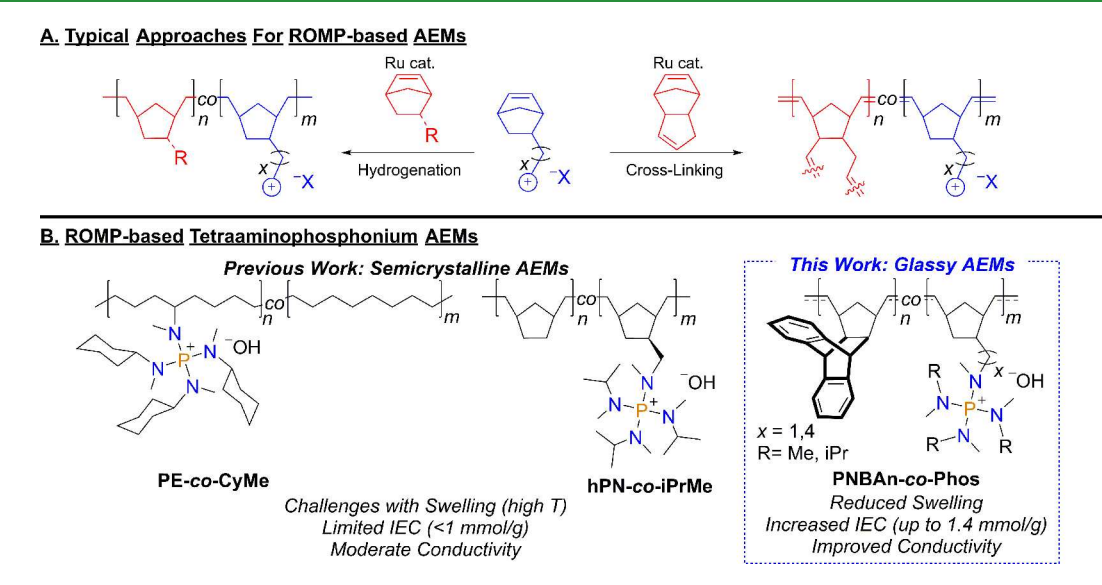


Figure 1. (A) Typical synthetic approaches to AEMs using ROMP and (B) tetraaminophosphonium AEMs prepared using ROMP.

Scheme 1. Preparation of Tetraaminophosphonium AEMs

$$PCl_{5} = \underbrace{\begin{array}{c} 1. \ RN(H)Me, \ NEt_{3} \\ 2. \ MeNH_{2} \\ C_{6}H_{5}Cl, \ 22^{\circ}C \\ 3. \ KPF_{6} \ workup \\ R = Me, \ iPr \end{array}}_{R} \underbrace{\begin{array}{c} 2.5 \ equiv. \\ NBAn \ (exo) \\ NB$$

demonstrates that simple modification of the poly(vinylene-1,3-cyclopentylene) backbone can be used to enhance the performance of polynorbornene-based AEMs.

■ RESULTS AND DISCUSSION

Preparation of Phosphonium Copolymers. Homopolymerization of NBAn (Scheme 1) using ROMP affords a rigid polymer with a $T_{\rm g}$ of 265 °C, which is a remarkable increase when compared to the $T_{\rm g}$ of 37 °C of the parent ring-opened polynorbornene. Here, NBAn was copolymerized with two different tetraaminophosphonium norbornenes using the Grubbs 3rd generation catalyst (Scheme 1). 5-(4-Bromobutyl)norbornene (NB-5-BuBr) was used as the synthetic precursor to the phosphonium monomers, as it can prepared in one step from the Diels—Alder cycloaddition of 6-bromo-1-hexene and cyclopentadiene. Displacement of the bromide with either $(Me_2N)_3P=NMe$ or $(Me(iPr)N)_3P=NMe$ enabled preparation of the two desired cationic monomers (Scheme 1). Tetraaminophosphonium cations were used here for AEM synthesis due to their exceptional alkaline stability. $^{33-35}$

Copolymerization of the NBAn and phosphonium-functionalized norbornenes was accomplished using 0.2 mol % of a ruthenium alkylidene catalyst in 1,2-dichloroethane to target

copolymers with degrees of polymerization of 500 ($DP_n = 500$). Copolymerizations of NBAn with either NB-5-BuP-(NMe₂)₃ or NB-5-BuP(N(iPr)Me)₃ were complete within 5 min, and the reactions were quenched with ethyl vinyl ether to deactivate the catalyst, followed by precipitation of the copolymers using diethyl ether. The isolated copolymers were soluble in 1,2-dichloroethane and 1,1,2,2-tetrachloroethane, but opaque solutions were obtained in other common organic solvents including CHCl₃, CH₂Cl₂, tetrahydrofuran (THF), dimethylacetamide, dimethylformamide (DMF), chlorobenzene, 1,2-dichlorobenzene, and methanol. Exchanging the counterion to Cl⁻ afforded improved solubility in DMF and methanol.

Examination of different comonomer compositions revealed that a 60:40 copolymer of the NBAn and phosphonium monomer was optimal to balance WU and hydroxide conductivity in these materials (Figure S17). Given this, the 60:40 copolymers were the primary focus of the work. Molecular weight analysis using gel permeation chromatography (GPC) of 60:40 PNBAn-co-iPrMe[PF $_6$] was possible in a 10 mM LiNTf $_2$ /THF eluent. ^{36,37} A fairly broad GPC trace was noted for this polymer under these conditions, and significant tailing at long elution times was observed as shown in Figure S16 ($M_n = 33 \text{ kg/mol}$, D = 1.50). These results were

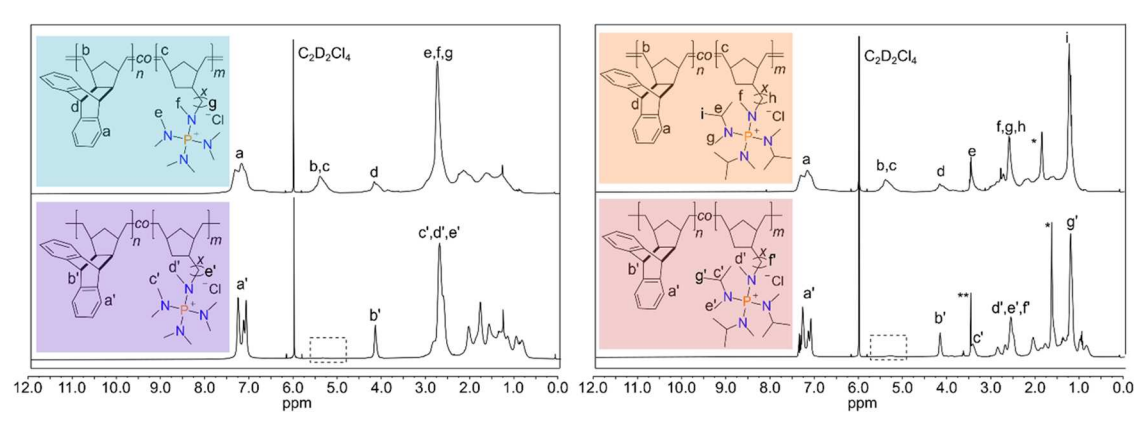


Figure 2. ¹H NMR spectra of 60:40 PNBAn-co-Me₂[CI] (left) and 60:40 PNBAn-co-iPrMe[CI] (right) before and after hydrogenation. All spectra were collected in tetrachloroethane- d_2 at 22 °C. The * signal is residual water, and the ** signal is residual methanol. The dotted box illustrates saturation of double bonds (\geq 95%).

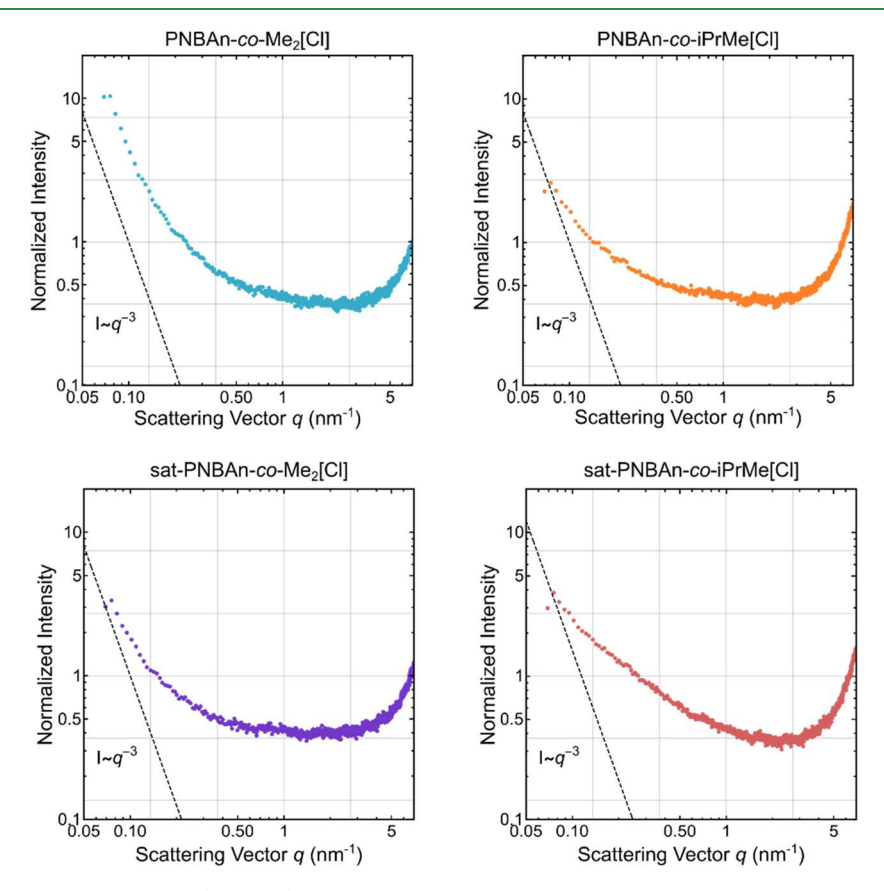


Figure 3. Invariant normalized SAXS profiles (log scale) of 60:40 PNBAn-co-Me₂[Cl] and 60:40 PNBAn-co-iPrMe[Cl] collected at 22 °C in tall narrow slit collimation geometry, before (top) and after (bottom) hydrogenation. The dashed lines were included as a reference to ideal Porod scaling which, for this geometry, can be approximated as $I-q^{-3.59}$ Linear scale SAXS profiles are shown in Figure S20.

surprising when compared to our prior work on ring-opened norbornenes, where recorded molecular weights were higher, and molecular weight distributions were narrower. It is possible that interactions between PNBAn-co-iPrMe[PF₆] and the stationary phase could be occurring, as the refractive index signal never returns to baseline at the end of the measurement (Figure S16). This was noted over repeated runs, suggesting that the molecular weight analysis in this instance can be considered at best, a rough estimate. No refractive index signal was noted for 60:40 PNBAn-co-Me₂[PF₆] when GPC analysis was attempted in 10 mM LiNTf₂/THF, despite our observation that both NBAn and NB-5-Bu(PNMe₂)₃ are

completely consumed during copolymerization. The poor solubility of the phosphonium copolymers in THF may contribute to the challenges in molecular weight determination, as both polymers dissolved in THF resulted in slightly turbid solutions. Nevertheless, this analysis provided some information on molecular weight unlike attempted GPC analysis in CHCl₃ or LiBr/DMF.

The proton nuclear magnetic resonance (¹H NMR) spectra collected for the 60:40 PNBAn-co-Me₂[Cl] and PNBAn-co-iPrMe[Cl] copolymers are shown in Figure 2. The broad signals observed for the unsaturated materials are partially a consequence of the restricted chain motion with the double

bonds in the backbone, in addition to the mixture of *cis* and *trans* configurations for these groups. Hydrogenation of the copolymers using *p*-toluenesulfonyl hydrazide resulted in ≥95% saturation of the double bonds,³⁸ with a narrowing of the ¹H NMR signals for the copolymers (Figure 2). The comonomer ratio in the polymer backbone is within a few percent of the targeted values as determined by comparison of the integrals for the *N*-alkyl signals from the tetraaminophosphonium cation to the benzyl protons of the anthracenyl side group (Supporting Information). We have noted improved accuracy in integration with the saturated copolymers, which was attributed to the narrower signals observed in these spectra (Figure 2).

Attempts to examine the relative rates of comonomer insertion were difficult in these copolymerizations, as the reactions were >90% complete after only 1 min. ¹H NMR spectra of aliquots removed from the reaction mixture confirmed that the sharp signals for the monomers (between 6.1 and 5.9 ppm) had disappeared and had been replaced by broad signals corresponding to the polymer backbone alkene groups (5.8–5.0 ppm). The long butyl tether ensures that polymerization of the *endo* phosphonium norbornene is rapid, which is notable given that *exo* monomers tend to display higher reactivity in ROMP. In the past, we have had difficulty polymerizing *endo* isomers of norbornene phosphoniums when the linker is short (methylene), ¹⁰ suggesting that the tether length may potentially be used as a tool to control composition along the chain.

The absence of distinct Bragg features in the small-angle X-ray scattering (SAXS) patterns for the PNBAn-co-Me₂[Cl] or PNBAn-co-iPrMe[Cl] copolymers (Figure 3) in the dry state (Cl⁻ form) suggested that ionic groups were not clustered along the backbone, as expected given the statistical nature of the copolymerization. Some increase of scattering intensity in the mid-q range (0.1–1 nm⁻¹) was observed for PNBAn-co-iPrMe[Cl] after hydrogenation, which hints at the enhancement of local packing density fluctuations, possibly indicating reordering facilitated by the concomitant increase of segmental mobility of the polymer backbone. The lack of phase separation was considered to be a benefit, as we have noted in norbornene-based phosphonium copolymers with bulky cationic groups that samples with distinct phase separation had higher WU and were more difficult to manipulate. $^{\rm 10}$

Differential scanning calorimetry (DSC) and thermo gravimetric analysis (TGA) were used to examine the thermal properties of the newly synthesized ring-opened polynorbornenes. It has been noted that counterions can have a large impact on the measured glass transition temperatures (T_{σ}) of polyelectrolytes. 40,41 In an effort to separate counterion effects from comonomer effects, we converted the PNBAn-coiPrMe[Cl] copolymer to the PNBAn-co-iPrMe[NTf₂] form, as the large bis(trifluoromethane)sulfonimide counterion (^NTf₂) does not seem to significantly impact $T_{\rm g}$ measurements in polyelectrolytes. ^{40,41} The measured $T_{\rm g}$ for PNBAn-coiPrMe[NTf₂] as determined from DSC scans was 150.7 °C (Figure 4). Saturation of the double bonds results in a reduction of the T_g to 133.6 °C (Figure 4), as expected.²⁸ This is in sharp contrast to PNBAn-co-iPrMe[Cl] where no T_g value was observed from 0 to 200 °C, demonstrating the importance of counterion choice in $T_{\rm g}$ measurements.

Copolymerization of NBAn with the butyl norbornene derivatives had the intended effect, as the decreased molecular mobility from the rigid anthracenyl unit leads to a T_{σ} well

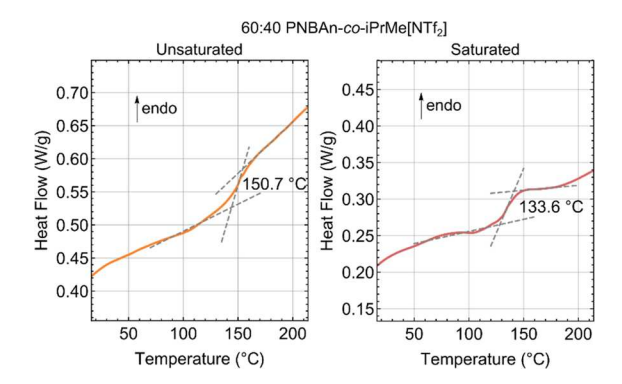


Figure 4. DSC traces (scan rate 20 °C/min) from the 3rd heating cycle for unsaturated (left) and saturated (right) 60:40 PNBAn-co-iPrMe[NTf₂] copolymers annotated with $T_{\rm g}$ values determined from the maxima of the first derivatives of heat flow versus temperature.

above that of the parent ring-opened polynorbornene ($T_{\rm g}$ = 37 and 4 °C for unsaturated and saturated, respectively). The $T_{\rm g}$ values for PNBAn-co-iPrMe[NTf₂] fall nearly halfway between the PNBAn homopolymer (265 and 221 °C) and poly(n-butylnorbornene) (8 and 1 °C). TGA studies revealed a two-step decomposition process for both saturated and unsaturated PNBAn-co-iPrMe[NTf₂], with nearly identical $T_{\rm d5\%}$ values of ~320 °C.

WU and Hydroxide Conductivity of the Phosphonium Polymers. Transparent thin films of the phosphonium copolymers (Cl⁻ form) were obtained by solution casting from 1,2-dichloroethane in stainless-steel Petri dishes at room temperature for 5 h. Films were typically manipulated when wet as they were ductile when hydrated; however, the films became brittle upon drying which precluded more in-depth mechanical property analysis. These copolymers were converted into the ⁻OH form for conductivity studies using electrochemical impedance spectroscopy (EIS) and WU measurements using gravimetric analysis (Table 1).

The unsaturated PNBAn-co-iPrMe[OH] and PNBAn-co-Me₂[OH] copolymers had lower WUs and were more conductive than a related ring-opened norbornene phosphonium at 80 °C (hPN-co-iPrMe[OH] shown in Figure 1B). The OH conductivity of PNBAn-co-iPrMe[OH] at 80 °C (50 mS/cm) was 25% higher than the comparable polymer without the anthracene side group (Table 1, entries 1–2). Moreover, a reduction in WU (from 75 to 65%) and hydration number (from 42 to 31) was noted for PNBAn-co-iPrMe[OH]. The OH conductivity at 80 °C was even higher with the smaller dimethylaminophosphonium cation tethered to the polymer backbone (Table 1, entry 3), highlighting the benefits of the smaller cation combined with the NBAn comonomer.

Both saturated copolymers had WUs within 10% of their unsaturated counterparts (Table 1, entries 4–5). Notably, upon hydrogenation of the double bonds, conductivity decreases for both copolymers at 80 °C, suggesting that higher molecular mobility may cause issues for anion transport in this case. To probe the impact of backbone saturation in more detail, a conductivity vs time experiment was carried out at 80 °C over 30 min using saturated and unsaturated 60:40 PNBAn-co-iPrMe[OH] (Figure 5). A 3 mS/cm loss in conductivity was noted for the unsaturated polymer, and 5 mS/cm loss is noted for the saturated copolymer. We suspect that differences in polymer backbone relaxation between the saturated and unsaturated materials influence the conductivity

Table 1. Optimized AEMs and Relevant Properties

entry	copolymer (monomer ratio)	$IEC_{theo}^{a} (mmol/g)$	IEC ^b (mmol/g)	WU ^c −OH (%)	λ^d	$\sigma_{25~^{\circ}\text{C}}^{e}$ OH (mS/cm)	$\sigma_{80~^{\circ}\text{C}}^{e}$ $^{-}\text{OH} (\text{mS/cm})$
1	hPN-co-iPrMe (86:14)	1.00	0.99	75	42	22 ± 1	40 ± 3
2	PNBAn-co-iPrMe (60:40) ^f	1.18	1.16	65	31	23 ± 2	50 ± 4
3	PNBAn-co-Me ₂ (60:40) ^f	1.37	1.24	56	25	29 ± 3	60 ± 7
4	PNBAn-co-iPrMe $(60:40)^g$	1.18	1.11	63	32	21 ± 2	39 ± 3
5	$PNBAn-co-Me_2$ (60:40) ^g	1.37	1.21	61	28	25 ± 3	55 ± 2
6	PNBAn-co-iPrMe (60:40) ^{fh}	1.21	0.90	49	30	30 ± 3	61 ± 4
7	PNBAn-co-NMe ₃ $(60:40)^f$	1.59	1.40	46	18	26 ± 4	56 ± 8
8	PNBAn-co-NMe ₃ $(50:50)^f$	2.02	1.72	75	24	52 ± 3	112 ± 9

^aTheoretical ion-exchange capacity values were determined from percent of the ionic group according to ¹H NMR. ^bIon exchange capacity was measured using standard back-titration methods. ¹⁰ ^cWater uptake (WU) was determined gravimetrically for each film in the ⁻OH form. ^dHydration values were calculated according to the equation $\lambda = [1000 \times \text{WU}]/[\text{IEC} \times 18]$. ^eConductivity was determined using electrochemical impedance spectroscopy (average of three trials with error corresponding to standard deviation). ^fUnsaturated polymer. ^gSaturated polymer. ^hMethylene tethered cation.

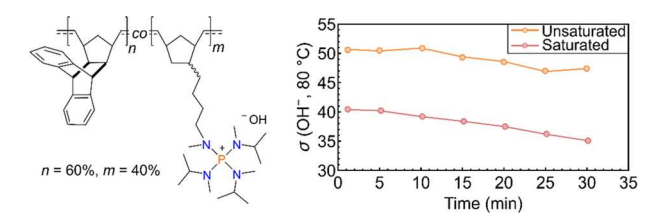


Figure 5. Hydroxide conductivity versus time for 60:40 PNBAn-co-iPrMe[OH] at 80 $^{\circ}$ C.

over time. This is consistent with other reports where backbone relaxation can lead to conductivity changes in polyelectrolytes. 42,43

Alkaline Stability. Cation and backbone stability toward hydroxides are arguably the most important features of any high-performing AEMs. Two approaches were used here to offer insight into stability of these phosphonium polymers. First, two small-molecule analogues of the cations ([P-(NMe₂)₄][Cl] and [P(N(iPr)Me)₄][Cl]) were mixed with 50% (w/w) NaOH/H₂O in phase-transfer reactions to rapidly quantify cation degradation with excess hydroxides. These studies mirror our prior work on cation degradation in alkaline media.³³ In addition to the small-molecule studies, the

copolymers were immersed in 10 M KOH at 80 $^{\circ}$ C to examine alkaline stability, similar to prior work by Holdcroft and co-workers who demonstrated the exceptional stability of benzimidazolium polymers. 44

Both $[P(NMe_2)_4][Cl]$ and $[P(N(iPr)Me)_4][Cl]$ were dissolved in C_6H_5Cl (0.04 M) and combined with 300 equiv of NaOH (50 wt % solution) to examine degradation with excess ${}^{-}$ OH. We have demonstrated previously that $[P(N-(iPr)Me)_4][Cl]$ degrades rapidly under these conditions at 100 ${}^{\circ}$ C. This likely happens via ${}^{-}$ OH attack at phosphorus forming a 5-coordinate intermediate, followed by deprotonation with a second equivalent of ${}^{-}$ OH to form the P=O bond, with elimination of an amino group. Since the temperature has a significant impact on the cation degradation rate in phase-transfer reactions, we re-examined $[P(N(iPr)Me)_4][Cl]$ degradation with >300 equiv of NaOH at 60 ${}^{\circ}$ C rather than 100 ${}^{\circ}$ C, which offers better comparison with literature reports (Figure S23).

In 3 h at 60 °C, 11% of $[P(N(iPr)Me)_4][Cl]$ had been converted to the relevant oxide, $O=P(N(iPr)Me)_3$, corresponding to a $t_{1/2} \sim 19$ h assuming a pseudo 1st order reaction. This is particularly impressive when benchmarked against quaternary ammonium salts typically used for phase-transfer

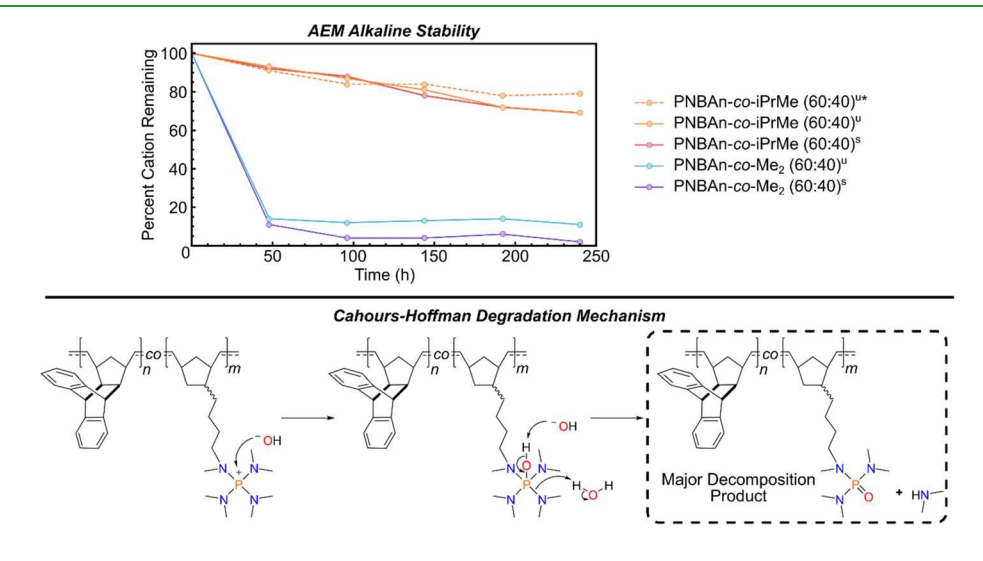


Figure 6. Top: Cation degradation for the PNBAn-co-Phos materials (u = unsaturated polymer, s = saturated polymer and * = Methylene tethered cation) was examined by immersing the solid polymers in 10 M KOH $_{aq}$ and periodically removing some sample from the vessel. The sample was dissolved in tetrachloroethane- d_2 for 31 P{ 1 H} NMR analysis where percent cation remaining was determined by comparing the ratio of the starting material to decomposition products. Bottom: Proposed cation decomposition mechanism for PNBAn-co-Me $_2$ [OH].

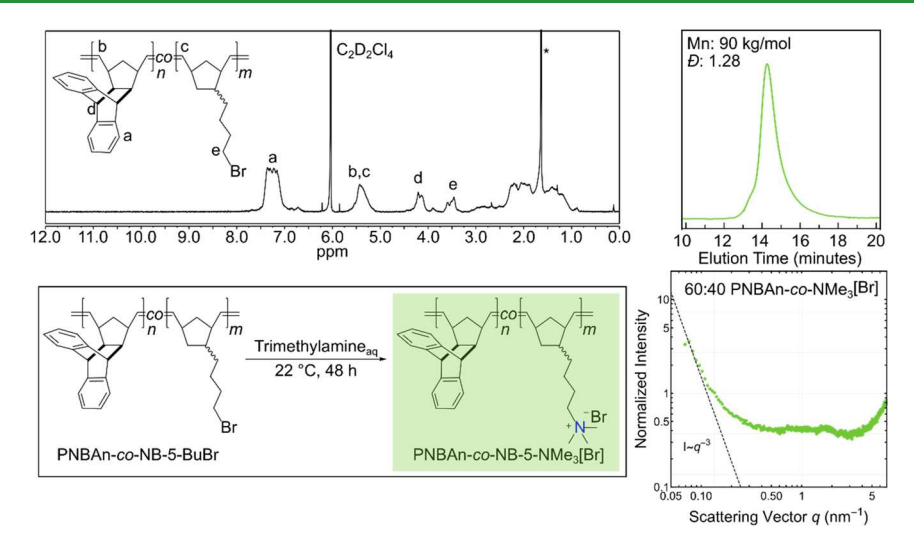


Figure 7. Top: 1 H NMR spectrum of 60:40 PNBAn-co-NB-5-BuBr (* corresponds to $H_{2}O$) and GPC trace of 60:40 PNBAn-co-NB-5-BuBr (molecular weight determined relative to the polystyrene standard). Bottom: Synthesis of 60:40 PNBAn-co-NMe $_{3}[Br]$. Invariant normalized SAXS profile of 60:40 PNBAn-co-NMe $_{3}[Br]$ collected at 22 $^{\circ}$ C in tall narrow slit collimation geometry.

catalysis, where tetrahexylammonium chloride $[N(C_6H_{13})_4]$ -[Cl] has a $t_{1/2}$ of 0.4 h under near identical conditions. ⁴⁶ In our hands, the smaller $[P(NMe_2)_4][Cl]$ cation completely oxidized to $O=P(NMe_2)_3$ in $C_6H_6Cl/50$ wt % NaOH at 60 °C after 1 h. It also degraded rapidly in 1 h at 22 °C (83%), corresponding to a $t_{1/2}$ of only 0.4 h at room temperature. This large stability difference between $[P(NMe_2)_4][Cl]$ and $[P(N(iPr)Me)_4][Cl]$ highlights the importance of the isopropyl group to limit direct attack at the phosphorus atom in tetraaminophosphoniums.

Submerging the synthesized PNBAn-co-Phos materials in 10 M KOH_{aq} at 80 °C produced a similar outcome to the phasetransfer reactions, where the larger phosphonium cation in PNBAn-co-iPrMe[OH] degraded much more slowly than the smaller analogue in PNBAn-co-Me₂[OH] (Figure 6). Approximately 30% of the cationic sites had degraded after 240 h for PNBAn-co-iPrMe[OH], while ~85% of the cationic sites had degraded in PNBAn-co-Me₂[OH] after just 48 h under the same conditions. Diagnostic signals for the oxide products $((R(R')N)_3P=O)$ were observed in the $^{31}P\{^1H\}$ NMR spectra $(\sim 26-24 \text{ ppm})$, indicating that oxide formation was the major mode of degradation (presumably through direct attack at phosphorus), similar to the small-molecule studies. Two oxide signals were observed in the degradation studies of both polymers, which is tentatively attributed to the unsymmetrical substitution pattern around the tetraaminophosphonium (Figures S28 and S29). Interestingly, a minor degradation product was also observed in the ³¹P{¹H} NMR spectrum for PNBAn-co-iPrMe[OH] copolymers after 240 h, which was attributed to a small amount of dealkylation (roughly 5–10%).

We reasoned that stability could be improved by bringing the phosphonium cation closer to the polymer chain, and this prediction proved to be accurate, with only 21% of the cation lost if the butyl tether is shortened to a methylene group (Figures 6 and S30). This is consistent with increased steric congestion around the phosphorus atom, making direct attack with the $^{-}$ OH anion more difficult. The $^{-}$ OH conductivity of this polymer is $\sigma = 61$ mS/cm at 80 $^{\circ}$ C, which is one of the highest measured (Table 1, entry 6) and \sim 50% higher than the hPN-co-iPrMe under the same conditions.

Chemical Aging. The phosphonium copolymers became markedly more brittle and difficult to handle after 240 h in 10

M KOH at 80 °C, making additional conductivity studies impossible. To determine whether this loss of mechanical integrity was attributed to cation degradation, we carried out a similar alkaline stability experiment to the one described above but at a lower concentration of KOH. Both saturated and unsaturated PNBAn-co-iPrMe[OH] were immersed in 5 M KOH for 240 h at 80 °C. Over that time, no appreciable degradation of the cation was observed, but the mechanical integrity of the polymers still deteriorated. GPC analysis revealed a molecular weight reduction from the initial value of 33 to 8 kg/mol for the unsaturated polymer and 17 kg/mol for the saturated derivative (Figure S33). As ring-opened norbornenes are susceptible to oxidative degradation, 47 suggests that part of the aging process can be attributed to backbone oxidation over time, leading to the reduction in molecular weight. One might expect to observe new signals in IR upon oxidation, but only subtle changes are noted in the IR spectrum for unsaturated PNBAn-co-iPrMe[Cl] after aging (Figure S35). The area where one would expect to see new carbonyl signals (1550-1700 cm⁻¹) also overlaps with the bending mode for water (~1650 cm⁻¹), making it difficult to get more information from this analysis (Figure S35). Further assessment of the aged polymers using NMR spectroscopy and SAXS (Figures S31, S32 and S34) did not provide additional insight into the decomposition pathway, but the GPC analysis over time clearly illustrated that the reduction in molecular weight contributes to embrittlement of the polymer.

Hydrogenation is a natural approach to limit polymer backbone oxidation, but we still observed embrittlement of the saturated copolymers in the 5 M and 10 M KOH studies. Residual double bonds are present in the hydrogenated copolymers using the tosyl hydrazide method, and an exhaustive hydrogenation would be key for future studies. We suspect that chemical aging causes issues with repeated conductivity measurements over time, as we have noted that σ values can decrease by 10% upon remeasuring using EIS. It should be noted that all reported values in Table 1 are the initial conductivity values measured for each material.

Trimethylammonium Copolymers. Finally, NBAn was copolymerized with NB-5-BuBr followed by treatment with NMe₃ to afford a trimethylammonium AEM (PNBAn-co-

NMe₃[Br]) for direct comparison with the phosphonium copolymers. Copolymerization of NBAn and NB-5-BuBr with the 0.2 mol % Grubbs 3rd generation catalyst was rapid at room temperature, and the 60:40 copolymer had an $M_{\rm n}$ = 90 kg/mol (Figure 7).

The neutral NBAn/NB-5-BuBr copolymer could be cast into a free-standing film from CHCl₃, and conversion to the desired PNBAn-co-NMe₃[Br] was accomplished by placing the solid film in 25 wt % aqueous NMe₃ for 2 days at 22 °C. The resultant PNBAn-co-NMe₃[Br] copolymers were insoluble in organic solvents, but IEC measurements suggested good conversion of the alkyl bromide groups to ammonium bromide groups (Table 1, entries 7 and 8). Phase separation was noted in the SAXS patterns for the PNBAn-co-NMe₃[Br] copolymers at ~2 nm⁻¹, which was attributed to ionic clustering in the film (Figure 7). This contrasts with the phosphonium AEMs, where no phase separation was observed, likely due to the larger more hydrophobic phosphonium cation.

For the 60:40 PNBAn-co-NMe₃[OH], conductivity was comparable to the 60:40 PNBAn-co-Me₂[OH]. Since the ammonium copolymer has a higher experimental IEC (1.4 to 1.24, Table 1 entry 7), this may suggest that percolation pathways are improved with the larger cation. However, the concentration of the phosphonium cation cannot be increased beyond 40 mol % due to excessive swelling. By contrast, the WU for a 50:50 PNBAn-co-NMe₃[OH] copolymer was only 75%, with a $\sigma_{80~^{\circ}\text{C}}$ = 112 ± 9 mS/cm (Table 1, entry 8). This demonstrates the benefits of the smaller cation, where IEC can be significantly increased to improve performance without excessive swelling in aqueous environments (Figure S18). The conductivity values for PNBAn-co-NMe₃[OH] compare well with prior reports on ammonium-functionalized ring-opened polynorbornenes, 15,20 as well as our prior report on high T_g ammonium-functionalized vinyl addition polynorbornenes.

The alkaline stability of 50:50 PNBAn-co-NMe₃[OH] was evaluated in 10 M KOH at 80 °C for comparison with the PNBAn-co-Phos AEMs. Surprisingly, the ammonium copolymer was still ductile after 2 days which enabled assessment of $^{-}$ OH conductivity. σ_{25} °C was 8 mS/cm, which was an 85% reduction compared to the initial value (Figure S36). We suspect that the ammonium cation degrades under these conditions, but NMR spectroscopy could not be used to confirm this degradation pathway since the copolymer was insoluble. After 4 days in 10 M KOH at 80 °C, the membrane became too brittle to manipulate, limiting further $^{-}$ OH conductivity measurements.

CONCLUSIONS

In conclusion, we have demonstrated that fusion of an anthracene moiety to the ring-opened polynorbornene backbone can improve AEM performance. The combination of the anthracenyl side group and double bonds along the polymer backbone limits WU and enables increased incorporation of large cationic groups. Though the additional rigidity from backbone double bonds is beneficial for conductivity measurements at 80 °C, chemical aging over time is a concern. Future work will focus on strategies to mitigate backbone oxidation while retaining a rigid-backbone framework.

The choice of the dialkylamino group around the phosphonium center was also examined and shown to impact both performance and stability. AEMs where the phosphonium center is surrounded by only dimethylamino groups are highly conductive but can be more susceptible to hydroxide

degradation. The use of isopropylmethylamino groups in place of dimethylamino groups markedly improves the chemical stability of the material, suggesting that secondary alkyl groups are key to the stability of tetraaminophosphonium cations, as shown previously.³⁴ The combination of polymer stability studies and model compound investigations in phasetransfer studies were key to identifying the degradation mechanisms in the materials and will be used in the future with novel cations in AEMs. Functionalization of these high $T_{\rm g}$ polymers with the benchmark trimethylammonium cation also provided insight into how cation size impacts OH transport and swelling when contrasted against phosphonium-based AEMs. Future studies will seek to implement rational design principles to facilitate high concentrations of bulky cations in AEMs with an improved balance of ion transport and swelling in water.

■ EXPERIMENTAL SECTION

Materials and Methods. Reagents and solvents were purchased from commercial sources and used as received. Grubbs' thirdgeneration catalyst or G3 ((H₂IMes)(pyr)₂(Cl)₂Ru=CHPh) was prepared according to a prior report. So 5-(4-Bromobutyl)-2-norbornene (NB-5-BuBr) and norbornene anthracene cycloadduct (NBAn) were prepared according to literature procedures. S2,49,51–53 Final purification of NBAn was accomplished via sublimation at 110 °C in vacuo. Tris(isopropyl(methyl)amino)(methylamino)-phosphonium hexafluorophosphate(V) and ((bicyclo[2.2.1]hept-5-en-2-ylmethyl)(methyl)amino) tris(isopropyl(methyl)amino)-phosphonium hexafluorophosphate(V) were prepared according to our previous report. 10

NMR Analysis. All NMR spectra were recorded on a 500 MHz Bruker Avance 3 spectrometer or a 500 MHz Bruker Neo spectrometer with Prodigy Cryoprobe. The $^1\mathrm{H}$ NMR spectra were referenced to residual protio solvents (7.26 ppm for CHCl3 and 6.00 ppm for TCE-d2), and $^{13}\mathrm{C}$ NMR spectra were referenced to the solvent signal (CDCl3: 77.2 ppm; TCE-d2: 73.8 ppm). The $^{31}\mathrm{P}\{^1\mathrm{H}\}$ NMR spectra were referenced to the lock signal. The example $^1\mathrm{H}$ NMR data for the phosphonium polymers is reported in the $^-\mathrm{PF}_6$ form in the experimental section below, while all the spectra included in the Supporting Information were recorded in the $^-\mathrm{Cl}$ form. The $^1\mathrm{H}$ NMR chemical shifts for these polymers are essentially the same, regardless of the counterion.

Gel-Permeation Chromatography (GPC). GPC measurements were performed using a Waters Instrument equipped with a 2690 autosampler, a Waters 2414 refractive index detector, and two SDV columns (Porosity 1000 and 1,000,000 Å; Polymer Standard Services). The eluent (THF) was doped with 10 mM lithium bis(trifluoromethanesulfonyl)imide (flow rate of 1 mL/min, 40 °C). A 9-point calibration based on polystyrene standards (Polystyrene, ReadyCal Kit, Polymer Standard Services) was applied for determination of molecular weights. Both PNBAn-co-NB-5-BuBr and PNBAn-co-iPrMe[PF₆] were dissolved in THF and filtered through a 0.22 μm PTFE syringe filter before analysis. The phosphonium polymer samples were slightly turbid before and after filtration.

lon Exchange Capacity and Conductivity. IEC was measured using standard back titration methods and carried out according to our prior report, with gentle heating during exchange. ¹⁰ Conductivity measurements were also carried out like our prior work, with a Scribner membrane conductivity clamp and a Bio-Logic SP-150 potentiostat. ¹⁰

Small-Angle X-Ray Scattering. SAXS was performed on polymer films using an Anton Paar SAXSess mc2 with narrow-slit beam collimation. ¹⁰

Fourier Transform Infrared Spectroscopy (FTIR). FTIR spectroscopy was performed using a PerkinElmer Frontier FT-IR spectrometer with an attenuated total reflectance attachment containing a germanium crystal. Raw spectra were obtained over a

range of 4000–600 cm⁻¹ with 4 cm⁻¹ resolution and analyzed using Spectrum software (PerkinElmer).

Differential Scanning Calorimetry (DSC) and Thermogravimetric Analysis (TGA). DSC analysis was performed using a TA Instruments DSC Q20. Samples were scanned over a range of -50 to 220 °C at a rate of 20 °C/min under a N_2 atmosphere for 3 cycles. TGA was performed using a TA Instruments TGA Q50 under a N_2 atmosphere. Samples were heated from 50 to 800 °C at a rate of 10 °C/min

Tris(dimethylamino)(methylamino)phosphonium Hexafluorophosphate(V). This was prepared nearly identically to tris(isopropyl(methyl)amino)(methylamino)phosphonium hexafluorophosphate(V), as described previously. 10 Under N2, 88.5 mL of a dimethylamine solution (177 mmol, 2.0 M in THF) was added dropwise to PCl₅ (12.3 g, 59 mmol) in chlorobenzene (250 mL) at 0 °C. Then, triethylamine (32.9 mL, 236 mmol) was added dropwise over a period of 10 min, and the reaction mixture was warmed to room temperature and stirred for 17 h. The resultant [ClP(NMe₂)₃]Cl salt was then treated with 35.4 mL of a methylamine solution (71 mmol, 2.0 M in THF) and heated to 55 °C for 17 h. The reaction mixture was filtered, and the filtrate was concentrated in vacuo at 80 °C. The crude product was then diluted with 200 mL of CH_2Cl_2 , washed twice with a saturated KPF₆ solution (2 × 150 mL), and once with water (100 mL). The organic layer was dried with anhydrous sodium sulfate and concentrated. The resultant crude oil was diluted in 10 mL of CH2Cl2 and precipitated into diethyl ether (500 mL). The white solid was isolated by filtration and used without further purification (13.8 g, 69% yield). ¹H NMR (500 MHz, CDCl₃) δ 2.76 (d, J_{PH} = 9.9 Hz, 18H), 2.69 (dd, J = 12.3, 5.6 Hz, 3H), 2.66 (dd, J = 13.8, 9.7 Hz, 1H). $^{13}\text{C}\{^{1}\text{H}\}$ NMR (126 MHz, CDCl₃) δ 37.1 (d, $J_{PC} = 4.6 \text{ Hz}$), 28.1 (d, $J_{PC} = 1.3 \text{ Hz}$). ³¹P{¹H} NMR (202 MHz, CDCl₃) δ 42.5, -143.4 (sep, J_{PF} = 712 Hz).

Tetrakis (dimethylamino) phosphonium Hexafluorophosphate(V). Tris(dimethylamino) (methylamino)-phosphonium hexafluorophosphate(V) (1.0 g, 3.0 mmol), chlorobenzene (6.6 mL), 3.3 g of 50% (w/w) KOH_{aq}, and methyl iodide (4.26 g, 30 mmol) were combined in a 25 mL pressure flask at 60 °C for 48 h. The flask was cooled, and the mixture was diluted with 25 mL of water as well as 25 mL of CH₂Cl₂. The organic layer was separated, the aqueous layer was extracted with CH₂Cl₂ (2 × 25 mL), and the combined organic layers were washed with a saturated KPF₆ solution (3 × 25 mL) as well as water (25 mL). The combined organic layers were dried with anhydrous sodium sulfate and concentrated. The crude oil was precipitated into diethyl ether (100 mL), and the solid was collected (0.76 g, 72% yield). ¹H NMR (500 MHz, CDCl₃) δ 2.77 (d, $J_{\rm PH}$ = 9.7 Hz, 24H). ¹³C{¹H} NMR (126 MHz, CDCl₃) δ 37.7 (d, $J_{\rm PC}$ = 4.5 Hz). ³¹P{¹H} NMR (202 MHz, CDCl₃) δ 44.2, -143.4 (sep, $J_{\rm PF}$ = 712 Hz).

Monomer Synthesis. Either tris(dimethylamino)(methylamino)phosphonium hexafluorophosphate(V) (2.06 g, 6.1 mmol) or tris(isopropyl(methyl)amino)(methylamino)phosphonium hexafluorophosphate(V) (2.58 g, 6.1 mmol) was combined with 5-(4bromobutyl)norbornene (3.5 g, 15.3 mmol) in chlorobenzene (13 mL) in a round-bottom flask. Then, 13.0 g of 50% (w/w) KOH_{aq} was added to the reaction mixture, and the flask was heated to either 60 or 100 °C for 48 h. Synthesis of NB-5-Bu-P(NMe $_2)_3$ was accomplished at 60 °C and NB-5-Bu-P(N(iPrMe)Me)₃ at 100 °C. After 48 h, the reaction mixture was cooled to room temperature and transferred to a separatory funnel where it was diluted with 50 mL of water and 50 mL of CH₂Cl₂. The organic layer was separated, and the aqueous layer was extracted with CH_2Cl_2 (2 × 50 mL). The combined organic layers were washed with a saturated KPF₆ solution (3 × 50 mL) as well as water (50 mL), then dried with anhydrous sodium sulfate, and concentrated. The crude product was purified by precipitation into 200 mL of diethyl ether. A mixture of endo/exo isomers (~4:1 ratio) was isolated, but a full assignment for the exo could not be included since all of the signals could not be resolved. Yield of NB-5-Bu-P(NMe₂)₃ was 78% (2.3 g) and yield of NB-5-Bu-P(N(iPrMe)Me)₃ was 80% (2.8 g).

endo-NB-5-Bu-P(NMe₂)₃. ¹H NMR (500 MHz, CDCl₃) δ 6.11 (dd, $J_{\rm HH}$ = 5.8, 3.0 Hz, 1H, H²), 5.89 (dd, $J_{\rm HH}$ = 5.7, 2.9 Hz, 1H, H³), 2.93–2.84 (m, 2H, H¹¹), 2.77–2.71 (m, 2H, H¹, H⁴ these signals overlap with that of H¹².1³), 2.75 (d, $J_{\rm PH}$ = 9.7 Hz, 3H, H¹²), 2.74 (d, $J_{\rm PH}$ = 9.7 Hz, 18H, H¹³), 2.01–1.90 (m, 1H, H⁵), 1.83 (ddd, $J_{\rm HH}$ = 11.3, 9.0, 3.8 Hz, 1H, H⁶exo), 1.62–1.48 (m, 2H, H¹⁰), 1.43–1.18 (m, 4H, H³, H²), 1.18–0.98 (m, 2H, H³), 0.47 (ddd, $J_{\rm HH}$ = 11.3, 4.3, 2.5 Hz, 1H, H⁶endo). ¹³C{¹H} NMR (126 MHz, CDCl₃) δ 137.4 (s, C²), 132.3 (s, C³), 49.7 (s, C³), 49.3 (d, J = 4.6 Hz, C¹¹), 45.5 and 42.7 (s, 2C, C¹, C⁴), 38.8 (s, C⁵), 37.5 (d, J = 4.6 Hz, C¹²), 35.7 (d, J = 3.6 Hz, C¹³), 34.6 (s, C³), 32.5 (s, C⁶), 28.3 (d, J = 2.5 Hz, C¹⁰), 26.0 (s, C°). ³¹P{¹H} NMR (202 MHz, CDCl₃) δ 43.1, −144.4 (sep, $J_{\rm PF}$ = 712 Hz). exo-NB-5-Bu-P(NMe₂)₃. ¹H NMR (500 MHz, CDCl₃) δ 6.07 (dd, $J_{\rm HH}$ = 5.7, 3.1 Hz, 1H, H³), 6.01 (dd, $J_{\rm HH}$ = 5.7, 2.9 Hz, 1H, H²), 2.76 (d, $J_{\rm PH}$ = 9.5 Hz, 3H, H¹³), 2.74 (d, $J_{\rm PH}$ = 9.7 Hz, 18H, H¹³), 2.48 (br s, 1H, H⁴). ¹³C{¹H} NMR (126 MHz, CDCl₃) δ 136.9 (s, C³), 136.5 (s, C²), 46.5 and 42.0 (s, 2C, C¹, C⁴), 45.4 (s, C⁻), 38.8 (s, C⁵), 36.3 (s, C³), 33.1 (s, C⁶), 26.3 (s, C¹⁰).

endo-NB-5-Bu-P(N(iPrMe)Me)₃. ¹H NMR (500 MHz, CDCl₃) δ 6.11 (dd, $J_{\text{HH}} = 5.7$, 3.0 Hz, 1H, H²), 5.88 (dd, $J_{\text{HH}} = 5.8$, 2.9 Hz, 1H, H³), 3.56–3.43 (m, 3H, H¹⁴), 2.94–2.85 (m, 2H, H¹¹), 2.77–2.71 (m, 2H, H¹, H⁴ these signals overlap with that of H¹²), 2.73 (d, $J_{\text{PH}} = 9.8$ Hz, 3H, H¹²), 2.61 (d, $J_{\text{PH}} = 9.8$ Hz, 9H, H¹³), 2.00–1.90 (m, 1H, H⁵), 1.87–1.79 (m, 1H, H^{6exo}), 1.63–1.49 (m, 2H, H¹⁰), 1.44–1.18 (m, 4H, H⁷, H⁹ overlapping with H¹⁵), 1.22 (d, $J_{\text{HH}} = 6.9$ Hz, 18H, H¹⁵) 1.18–0.99 (m, 2H, H⁸), 0.47 (ddd, $J_{\text{HH}} = 11.3$, 4.4, 2.6 Hz, 1H, H^{6endo}). ¹³C{¹H} NMR (126 MHz, CDCl₃) δ 137.4 (s, C²), 132.3 (s, C³), 49.8 (s, C⁷), 49.6 (d, $J_{\text{PC}} = 4.3$ Hz, C¹¹), 47.2 (d, $J_{\text{PC}} = 5.8$ Hz, C¹⁴), 45.5 and 42.7 (s, 2C, C¹, C⁴), 38.8 (s, C⁵), 35.5 (d, $J_{\text{PC}} = 3.9$ Hz, C¹²), 34.6 (s, C⁸), 32.5 (s, C⁶), 28.6 (d, $J_{\text{PC}} = 3.6$ Hz, C¹³), 28.3 (d, $J_{\text{PC}} = 2.8$ Hz, C¹⁰), 26.1 (s, C⁹), 20.0 (d, $J_{\text{PC}} = 3.4$ Hz, C¹⁵). ³¹P{¹H} NMR (202 MHz, CDCl₃) δ 44.0, -144.4 (sep, $J_{\text{PF}} = 712$ Hz). exo-NB-5-Bu-P(N(iPrMe)Me)₃. ¹H NMR (500 MHz, CDCl₃) δ 6.07 (dd, $J_{\text{HH}} = 5.7$, 3.0 Hz, 1H, H³), 6.01 (dd, $J_{\text{HH}} = 5.7$, 2.9 Hz, 1H, H²), 2.80–2.77 and 2.50–2.47 (br s, 2H, H¹ and H⁴), 2.74 (d, $J_{\text{PH}} = 9.7$ Hz, 3H, H¹²), 2.62 (d, $J_{\text{PH}} = 9.8$ Hz, 9H, H¹³). ¹³C{¹H} NMR (126 MHz, CDCl₃) δ 136.9 (s, C³), 136.5 (s, C²), 46.5 and 42.0 (s, 2C, C¹, C⁴), 45.4 (s, C⁷), 38.8 (s, C⁵), 36.3 (s, C⁸), 33.2 (s, C⁶), 26.4 (s, C¹⁰).

General PNBAn-co-Phos Polymerization Procedure. Under N₂, NBAn (3.66, 3.30, or 2.75 mmol) and either NB-5-Bu-P(NMe₂)₃ or NB-5-Bu-P(N(iPrMe)Me)₃ (1.84, 2.2, or 2.75 mmol) were combined in a Schlenk flask with 218 mL of 1,2-dichloroethane. Then, 8.0 mg (0.011 mmol) of G3 (dissolved in 1.6 mL of 1,2dichloroethane) was rapidly injected into the reaction solution. Throughout the polymerization, no changes in viscosity were observed. After 5 min, 1.0 mL (10.4 mmol) of ethyl vinyl ether was rapidly injected into the mixture to quench the polymerization. The mixture was concentrated (~5 mL) and precipitated into 50 mL of diethyl ether. The precipitated product was isolated and dried in vacuo at 60 °C for 16 h (>80% yield). It should be noted that the integrals for the aliphatic region (2.5-0.5 ppm) did not match perfectly with the expected value. Example spectral data for unsaturated 60:40 PNBAn-co-Me₂[PF₆]: ¹H NMR (500 MHz, TCE- d_2) δ 7.65-6.45 (br m, 12H), 5.70-5.00 (br, 5H), 4.50-3.70 (br, 3H), 3.20-2.42 (br, 25H), 2.42-0.82 (br m, 20H). ³¹P{¹H} NMR (202 MHz, TCE- d_2) δ 44.0, -143.5 (sep, J_{PF} = 712 Hz). Example spectral data for unsaturated 60:40 PNBAn-co-iPrMe[PF₆]:

¹H NMR (500 MHz, TCE- d_2) δ 7.60–6.50 (br, 12H), 5.75–5.00 (br, 5H), 4.50–3.70 (br m, 3H), 3.65–3.25 (br, 3H), 3.15–2.40 (br m, 16H), 2.39–0.82 (br m, 38H). ³¹P{¹H} NMR (202 MHz, TCE- d_2) δ 44.8, –143.7 (sep, $J_{\rm PF}$ = 712 Hz).

General PNBAn-co-Phos Hydrogenation Procedure. The unsaturated PNBAn-co-Phos[Cl] copolymer (2.6 mmol double bonds), 2.46 g of p-toluene sulfonyl hydrazide (13.2 mmol), and 2.7 mL (14.5 mmol) of tripropylamine were combined in a roundbottom flask with 15 mL of 1:1 chlorobenzene/butanol and heated to 110 °C for 5 h. Then, the reaction mixture was concentrated to ~5 mL and precipitated into 50 mL of diethyl ether. The precipitate was isolated and soaked in 25 mL of a saturated KPF₆ methanol solution at 40 °C (3 × 1 h). The product was then soaked in 25 mL of methanol at 22 °C for 1 h and dried in vacuo at 60 °C for 16 h (>70% yield). Percent incorporation was determined by comparison of N-CH₃ and N-CH₂- signals (δ 3.13–2.34) which account for either 23H or 14H in the DiMe and iPrMe derivatives to the benzyl protons of the NBAn between 4.3 and 4.0 ppm. Example spectral data for saturated 60:40 PNBAn-co-Me₂[PF₆]: ¹H NMR (500 MHz, TCE-d₂) δ 7.50–6.88 (br m, 12H), 4.30–4.00 (br, 3H), 3.11–2.35 (br m, 23H), 2.31–0.61 (br m, 32H). $^{31}P\{^{1}H\}$ NMR (202 MHz, TCE- d_2) δ 43.9, -143.5 (sep, $J_{PF} = 712$ Hz). Example spectral data for saturated 60:40 PNBAn-co-iPrMe[PF₆]: 1 H NMR (500 MHz, TCE- d_2) δ 7.46– 6.90 (br m, 12H), 4.30-4.00 (br, 3H), 3.55-3.20 (br, 3H), 3.05-2.30 (br m, 14H), 2.3-0.6 (br m, 50H). ³¹P{¹H} NMR (202 MHz, TCE- d_2) δ 44.9, -143.6 (sep, J_{PF} = 712 Hz).

Anion Exchange of PNBAn-co-Phos [PF₆] to PNBAn-co-Phos[CI] Using an Amberlite IRA-400 CI⁻ Exchange Resin. First, 0.75 g of PNBAn-co-Phos[PF₆] was dissolved in 40 mL of a 1:1 1,2-dichloroethane/methanol solution and combined with 7.5 g of ion exchange resin for 17 h (this can be repeated as needed to ensure complete conversion of the counterion to chloride). After filtration, the solution was concentrated and precipitated in 50 mL of diethyl ether. The precipitate was isolated and dried to afford a white solid (>80% yield).

Anion Exchange of PNBAn-co-Phos[CI] to PNBAn-co-Phos-[NTf₂]. First, 0.075 g of PNBAn-co-Phos[CI] dissolved in 15 mL of 1,2-dichloroethane was washed with 1 M LiNTf₂ solution (3 × 30 mL) and water (3 × 30 mL). The organic phase was dried with sodium sulfate and then concentrated. The concentrate was precipitated into 50 mL of diethyl ether. The polymer was isolated and dried in vacuo at 60 °C for 4 h (0.052 g, 70% yield). The product was analyzed by $^{19}F\{^{1}H\}$ to ensure conversion of the counterion to NTf₂⁻. The ^{1}H NMR data are essentially identical to the $^{-}PF_{6}$ form. Example $^{19}F\{^{1}H\}$ spectral data for unsaturated 60:40 PNBAn-co-Me₂[NTf₂]: ^{19}F NMR (471 MHz) δ –79.2.

General Procedure for Degradation Using Phase-Transfer Chemistry. The phase-transfer stability study was carried out like in prior reports. ^{33,46} A phosphonium chloride salt (0.28 mmol) was weighed directly in a 20 mL scintillation vial and dissolved in chlorobenzene (7 mL, 0.04 M). Then, 7 g of a 50% w/w solution of NaOH_{aq} was added to the vial. After 1 min of stirring, an aliquot was removed from the organic layer and diluted with 0.6 mL of CD₂Cl₂ for an initial NMR analysis (t = 0 h). The vial was then heated to 60 °C with a stir rate of at least 800 rpm. At periodic intervals, the reaction mixture was cooled and a 50 μ L aliquot was removed from the organic layer, diluted with 0.6 mL of CD₂Cl₂, and analyzed using NMR spectroscopy. Percent cation remaining was determined by integration of all phosphorus signals present in the mixture and calculation of a ratio (NMR spectra in Figures S24–S27).

General PNBAn-co-NB-5-BuBr Polymerization Procedure. Under N₂, NBAn (2.88 or 2.40 mmol) and NB-5-BuBr (1.92 or 2.40 mmol) were combined in a 500 mL Schlenk flask and dissolved in 190 mL of 1,2-dichloroethane. Then, 7.0 mg (0.0096 mmol) of G3 (dissolved in 1.4 mL of 1,2-dichloroethane) was rapidly injected into the reaction solution. The reaction mixture was stirred for 5 min and was then quenched by rapidly injecting 1.0 mL (10.4 mmol) of ethyl vinyl ether followed by stirring for 30 min. The reaction was concentrated to approximately 5 mL and precipitated into 50 mL of methanol. The polymer was isolated and dried to afford a white solid

(>90% yield). Example spectral data for unsaturated 60:40 PNBAnco-NB-5-BuBr: 1 H NMR (500 MHz, CDCl₃) δ 7.50–6.55 (br, 12H), 5.65–5.05 (br, 5H), 4.40–3.95 (br, 3H), 3.65–3.25 (br, 2H), 3.10–2.40 (br, 2H), 2.38–1.78 (br, 10H), 1.77–0.91 (br, 10H). Integration for 1 H NMR signals reported relative to the methylene bromide signal (δ 3.65–3.25) being set to 2H.

General PNBAn-co-NB-5-BuBr Hydrogenation Procedure. The unsaturated PNBAn-co-NB-5-C₄H₈Br copolymer (2.0 mmol double bonds), 1.86 g of *p*-toluene sulfonyl hydrazide (10 mmol), and 10 mL of chlorobenzene were combined in a round-bottom flask and heated to 110 °C for 5 h. The solution was concentrated to ~5 mL and precipitated into 50 mL of methanol. The polymer was isolated and then rinsed with water (3 × 50 mL) and methanol (3 × 50 mL). The product was then dried at 60 °C in vacuo to afford a white solid (>70% yield). Example spectral data for saturated 60:40 PNBAn-co-NB-5-BuBr: 1 H NMR (500 MHz, CDCl₃) δ 7.32–7.02 (br m, 12H), 4.23–4.03 (br, 3H), 3.50–3.33 (br, 2H), 2.19–1.68 (br, 10H), 1.67–0.66 (br m, 22H). Integration for 1 H NMR signals reported relative to the methylene bromide signal (δ 3.50–3.33) being set to 2H.

General Procedure for Alkaline Stability in 10 and 5 M KOH. Membrane strips (\sim 20 × 5 × 0.05 mm) were soaked in 1 M KOH in a polypropylene bottle for 24 h. The KOH solution was decanted, and the strips were washed with 25 mL portions of deionized water (3 × 20 min). Membrane strips, now in the OH form, were submerged in 25 mL of 5 M or 10 M KOH in a PTFE bottle and heated to 80 $^{\circ}$ C in an oven. In the 10 M study, samples were removed every 48 h and washed with deionized water (3 × 20 min) before drying in vacuo at 22 °C for 17 h. The material was then dissolved in TCE- d_2 for NMR analysis. In the 5 M study, the polymer sample was removed from the alkaline solution after 240 h, washed, and treated with 0.1 M HCl solution for 17 h to convert the counterion to Cl-. The material was then washed with water $(3 \times 20 \text{ min})$ and dried before dissolution in TCE- d_2 for NMR analysis. For GPC, the polymer was dissolved in a minimal amount of 1,2-dichloroethane and precipitated from saturated methanol/KPF₆ solution to convert the polymer to the ${\rm PF_6}^-$ form. The precipitate was then isolated, dried, and analyzed.

ASSOCIATED CONTENT

Supporting Information

The Supporting Information is available free of charge at https://pubs.acs.org/doi/10.1021/acsapm.2c00297.

NMR spectra, GPC traces, thermal analysis (TGA and DSC), sample Nyquist plots, FTIR data, and additional SAXS analysis (PDF)

AUTHOR INFORMATION

Corresponding Authors

Tomasz Kowalewski – Department of Chemistry, Carnegie Mellon University, Pittsburgh, Pennsylvania 15213-2617, United States; o orcid.org/0000-0002-3544-554X; Email: tomek@andrew.cmu.edu

Kevin J. T. Noonan — Department of Chemistry, Carnegie Mellon University, Pittsburgh, Pennsylvania 15213-2617, United States; orcid.org/0000-0003-4061-7593; Email: noonan@andrew.cmu.edu

Authors

Jamie C. Gaitor – Department of Chemistry, Carnegie Mellon University, Pittsburgh, Pennsylvania 15213-2617, United States

Megan Treichel – Department of Chemistry, Carnegie Mellon University, Pittsburgh, Pennsylvania 15213-2617, United States

Complete contact information is available at: https://pubs.acs.org/10.1021/acsapm.2c00297

Author Contributions

All authors have given approval to the final version of the manuscript.

Notes

The authors declare no competing financial interest.

ACKNOWLEDGMENTS

J.C.G. is grateful to PPG and GEM for fellowships. This work was primarily supported by the National Science Foundation, under Grant No. CHE-1809658. A portion of the polymer stability studies were carried out under financial support from the Center for Alkaline-Based Energy Solutions (CABES), an Energy Frontier Research Center funded by the U.S. Department of Energy, Office of Science, Basic Energy Sciences under Award # DE-SC0019445. Bryan Pivovar (NREL) is also gratefully acknowledged for helpful discussions and Terry Collins (CMU) for help with pH measurements. Doowon Lee at the University of Pittsburgh is acknowledged for help with SAXS measurements, and Roberto Gil is acknowledged for help with NMR assignments with endo/exo monomers.

REFERENCES

- (1) Yang, Y.; Peltier, C. R.; Zeng, R.; Schimmenti, R.; Li, Q.; Huang, X.; Yan, Z.; Potsi, G.; Selhorst, R.; Lu, X.; Xu, W.; Tader, M.; Soudackov, A. V.; Zhang, H.; Krumov, M.; Murray, E.; Xu, P.; Hitt, J.; Xu, L.; Ko, H.-Y.; Ernst, B. G.; Bundschu, C.; Luo, A.; Markovich, D.; Hu, M.; He, C.; Wang, H.; Fang, J.; DiStasio, R. A.; Kourkoutis, L. F.; Singer, A.; Noonan, K. J. T.; Xiao, L.; Zhuang, L.; Pivovar, B. S.; Zelenay, P.; Herrero, E.; Feliu, J. M.; Suntivich, J.; Giannelis, E. P.; Hammes-Schiffer, S.; Arias, T.; Mavrikakis, M.; Mallouk, T. E.; Brock, J. D.; Muller, D. A.; DiSalvo, F. J.; Coates, G. W.; Abruña, H. D. Electrocatalysis in Alkaline Media and Alkaline Membrane-Based Energy Technologies. *Chem. Rev.* 2022, 122, 6117–6321.
- (2) Ramaswamy, N.; Mukerjee, S. Alkaline Anion-Exchange Membrane Fuel Cells: Challenges in Electrocatalysis and Interfacial Charge Transfer. *Chem. Rev.* **2019**, *119*, 11945–11979.
- (3) Dekel, D. R. Review of Cell Performance in Anion Exchange Membrane Fuel Cells. *J. Power Sources* **2018**, 375, 158–169.
- (4) Arges, C. G.; Zhang, L. Anion Exchange Membranes' Evolution toward High Hydroxide Ion Conductivity and Alkaline Resiliency. *ACS Appl. Energy Mater.* **2018**, *1*, 2991–3012.
- (5) Gottesfeld, S.; Dekel, D. R.; Page, M.; Bae, C.; Yan, Y.; Zelenay, P.; Kim, Y. S. Anion Exchange Membrane Fuel Cells: Current Status and Remaining Challenges. *J. Power Sources* **2018**, *375*, 170–184.
- (6) Hickner, M. A. Strategies for Developing New Anion Exchange Membranes and Electrode Ionomers. *Electrochem. Soc. Interface* **2017**, 26, 69–73.
- (7) Varcoe, J. R.; Atanassov, P.; Dekel, D. R.; Herring, A. M.; Hickner, M. A.; Kohl, P. A.; Kucernak, A. R.; Mustain, W. E.; Nijmeijer, K.; Scott, K.; Xu, T.; Zhuang, L. Anion-Exchange Membranes in Electrochemical Energy Systems. *Energy Environ. Sci.* **2014**, *7*, 3135–3191.
- (8) Wang, Y.-J.; Qiao, J.; Baker, R.; Zhang, J. Alkaline Polymer Electrolyte Membranes for Fuel Cell Applications. *Chem. Soc. Rev.* **2013**, 42, 5768–5787.
- (9) You, W.; Noonan, K. J. T.; Coates, G. W. Alkaline-Stable Anion Exchange Membranes: A Review of Synthetic Approaches. *Prog. Polym. Sci.* **2020**, *100*, No. 101177.
- (10) Treichel, M.; Womble, C. T.; Selhorst, R.; Gaitor, J.; Pathiranage, T. M. S. K.; Kowalewski, T.; Noonan, K. J. T. Exploring the Effects of Bulky Cations Tethered to Semicrystalline Polymers: The Case of Tetraaminophosphoniums with Ring-Opened Polynorbornenes. *Macromolecules* **2020**, *53*, 8509–8518.

- (11) Zhu, T.; Tang, C. Crosslinked Metallo-polyelectrolytes with Enhanced Flexibility and Dimensional Stability for Anion-Exchange Membranes. *Polym. Chem.* **2020**, *11*, 4542–4546.
- (12) Zhu, T.; Sha, Y.; Firouzjaie, H. A.; Peng, X.; Cha, Y.; Dissanayake, D. M. M. M.; Smith, M. D.; Vannucci, A. K.; Mustain, W. E.; Tang, C. Rational Synthesis of Metallo-Cations Toward Redoxand Alkaline-Stable Metallo-Polyelectrolytes. *J. Am. Chem. Soc.* **2020**, *142*, 1083–1089.
- (13) Yuan, H.; Liu, Y.; Tsai, T.-H.; Liu, X.; Kim, S. B.; Gupta, R.; Zhang, W.; Ertem, S. P.; Seifert, S.; Herring, A. M.; Coughlin, E. B. Ring-Opening Metathesis Polymerization of Cobaltocenium Derivative to Prepare Anion Exchange Membrane with High Ionic Conductivity. *Polyhedron* **2020**, *181*, No. 114462.
- (14) You, W.; Padgett, E.; MacMillan, S. N.; Muller, D. A.; Coates, G. W. Highly Conductive and Chemically Stable Alkaline Anion Exchange Membranes via ROMP of *trans*-Cyclooctene Derivatives. *Proc. Natl. Acad. Sci. U. S. A.* **2019**, *116*, 9729–9734.
- (15) Chen, W.; Mandal, M.; Huang, G.; Wu, X.; He, G.; Kohl, P. A. Highly Conducting Anion-Exchange Membranes Based on Cross-Linked Poly(norbornene): Ring Opening Metathesis Polymerization. ACS Appl. Energy Mater. 2019, 2, 2458–2468.
- (16) Zhu, T.; Xu, S.; Rahman, A.; Dogdibegovic, E.; Yang, P.; Pageni, P.; Kabir, M. P.; Zhou, X.-d.; Tang, C. Cationic Metallo-Polyelectrolytes for Robust Alkaline Anion-Exchange Membranes. *Angew. Chem., Int. Ed. Engl.* **2018**, *57*, 2388–2392.
- (17) You, W.; Hugar, K. M.; Coates, G. W. Synthesis of Alkaline Anion Exchange Membranes with Chemically Stable Imidazolium Cations: Unexpected Cross-Linked Macrocycles from Ring-Fused ROMP Monomers. *Macromolecules* **2018**, *51*, 3212–3218.
- (18) Kwasny, M. T.; Zhu, L.; Hickner, M. A.; Tew, G. N. Utilizing Thiol-Ene Chemistry for Crosslinked Nickel Cation-Based Anion Exchange Membranes. *J. Polym. Sci., Part A: Polym. Chem.* **2018**, *56*, 328–339.
- (19) Kwasny, M. T.; Zhu, L.; Hickner, M. A.; Tew, G. N. Thermodynamics of Counterion Release Is Critical for Anion Exchange Membrane Conductivity. *J. Am. Chem. Soc.* **2018**, *140*, 7961–7969.
- (20) Price, S. C.; Ren, X.; Savage, A. M.; Beyer, F. L. Synthesis and Characterization of Anion-Exchange Membranes Based on Hydrogenated Poly(norbornene). *Polym. Chem.* **2017**, *8*, 5708–5717.
- (21) Kwasny, M. T.; Tew, G. N. Expanding Metal Cation Options in Polymeric Anion Exchange Membranes. *J. Mater. Chem. A* **2017**, *5*, 1400–1405.
- (22) Disabb-Miller, M. L.; Zha, Y.; DeCarlo, A. J.; Pawar, M.; Tew, G. N.; Hickner, M. A. Water Uptake and Ion Mobility in Cross-Linked Bis(terpyridine)ruthenium-Based Anion Exchange Membranes. *Macromolecules* **2013**, *46*, 9279–9287.
- (23) Noonan, K. J. T.; Hugar, K. M.; Kostalik, H. A.; Lobkovsky, E. B.; Abruña, H. D.; Coates, G. W. Phosphonium-Functionalized Polyethylene: A New Class of Base-Stable Alkaline Anion Exchange Membranes. *J. Am. Chem. Soc.* **2012**, *134*, 18161–18164.
- (24) Zha, Y.; Disabb-Miller, M. L.; Johnson, Z. D.; Hickner, M. A.; Tew, G. N. Metal-Cation-Based Anion Exchange Membranes. *J. Am. Chem. Soc.* **2012**, *134*, 4493–4496.
- (25) Robertson, N. J.; Kostalik, H. A.; Clark, T. J.; Mutolo, P. F.; Abruña, H. D.; Coates, G. W. Tunable High Performance Cross-Linked Alkaline Anion Exchange Membranes for Fuel Cell Applications. *J. Am. Chem. Soc.* **2010**, *132*, 3400–3404.
- (26) Kostalik, H. A.; Clark, T. J.; Robertson, N. J.; Mutolo, P. F.; Longo, J. M.; Abruña, H. D.; Coates, G. W. Solvent Processable Tetraalkylammonium-Functionalized Polyethylene for Use as an Alkaline Anion Exchange Membrane. *Macromolecules* **2010**, 43, 7147–7150.
- (27) Clark, T. J.; Robertson, N. J.; Kostalik, H. A.; Lobkovsky, E. B.; Mutolo, P. F.; Abruña, H. D.; Coates, G. W. A Ring-Opening Metathesis Polymerization Route to Alkaline Anion Exchange Membranes: Development of Hydroxide-Conducting Thin Films from an Ammonium-Functionalized Monomer. *J. Am. Chem. Soc.* **2009**, *131*, 12888–12889.

- (28) Hatjopoulos, J. D.; Register, R. A. Synthesis and Properties of Well-Defined Elastomeric Poly(alkylnorbornene)s and Their Hydrogenated Derivatives. *Macromolecules* **2005**, *38*, 10320–10322.
- (29) Yang, J.-X.; Cui, J.; Long, Y.-Y.; Li, Y.-G.; Li, Y.-S. Synthesis of Cyclic Olefin Polymers with High Glass Transition Temperature by Ring-Opening Metathesis Copolymerization and Subsequent Hydrogenation. J. Polym. Sci. Part A. Polym. Chem. 2014, 52, 2654–2661.
- (30) Cui, J.; Yang, J.-X.; Pan, L.; Li, Y.-S. Synthesis of Novel Cyclic Olefin Polymer with High Glass Transition Temperature via Ring-Opening Metathesis Polymerization. *Macromol. Chem. Phys.* **2016**, 217, 2708–2716.
- (31) Choi, T.-L.; Grubbs, R. H. Controlled Living Ring-Opening-Metathesis Polymerization by a Fast-Initiating Ruthenium Catalyst. *Angew. Chem., Int. Ed.* **2003**, 42, 1743–1746.
- (32) Martínez-Arranz, S.; Albéniz, A. C.; Espinet, P. Versatile Route to Functionalized Vinylic Addition Polynorbornenes. *Macromolecules* **2010**, 43, 7482–7487.
- (33) Womble, C. T.; Kang, J.; Hugar, K. M.; Coates, G. W.; Bernhard, S.; Noonan, K. J. T. Rapid Analysis of Tetrakis-(dialkylamino)phosphonium Stability in Alkaline Media. *Organometallics* **2017**, *36*, 4038–4046.
- (34) Schwesinger, R.; Link, R.; Wenzl, P.; Kossek, S.; Keller, M. Extremely Base-Resistant Organic Phosphazenium Cations. *Chem. Eur. J.* **2006**, *12*, 429–437.
- (35) Marchenko, A. P.; Koidan, G. N.; Pinchuk, A. M. Reactions of Tetrakis(Dialkylamido)Phosphonium Bromides with Bases. *Russ. J. Gen. Chem.* **1984**, *54*, 2405–2409.
- (36) Womble, C. T.; Coates, G. W.; Matyjaszewski, K.; Noonan, K. J. T. Tetrakis(dialkylamino)phosphonium Polyelectrolytes Prepared by Reversible Addition-Fragmentation Chain Transfer Polymerization. *ACS Macro Lett.* **2016**, *5*, 253–257.
- (37) He, H.; Zhong, M.; Adzima, B.; Luebke, D.; Nulwala, H.; Matyjaszewski, K. A Simple and Universal Gel Permeation Chromatography Technique for Precise Molecular Weight Characterization of Well-Defined Poly(ionic liquid)s. J. Am. Chem. Soc. 2013, 135, 4227–4230.
- (38) Ai-Samak, B.; Amir-Ebrahimi, V.; Carvill, A. G.; Hamilton, J. G.; Rooney, J. J. Determination of the Tacticity of Ring-Opened Metathesis Polymers of Norbornene and Norbornadiene by ¹³C NMR Spectroscopy of Their Hydrogenated Derivatives. *Polym. Int.* **1996**, *41*, 85–92.
- (39) Roe, R. J., Methods of X-Ray and Neutron Scattering in Polymer Science. Oxford University Press: New York, 2000; p 331.
- (40) Hunley, M. T.; England, J. P.; Long, T. E. Influence of Counteranion on the Thermal and Solution Behavior of Poly(2-(dimethylamino)ethyl methacrylate)-Based Polyelectrolytes. *Macromolecules* **2010**, *43*, 9998–10005.
- (41) Cheng, S.; Zhang, M.; Wu, T.; Hemp, S. T.; Mather, B. D.; Moore, R. B.; Long, T. E. Ionic Aggregation in Random Copolymers Containing Phosphonium Ionic Liquid Monomers. *J. Polym. Sci., Part A: Polym. Chem.* **2012**, *50*, 166–173.
- (42) Vezzù, K.; Maes, A. M.; Bertasi, F.; Motz, A. R.; Tsai, T.-H.; Coughlin, E. B.; Herring, A. M.; Di Noto, V. Interplay Between Hydroxyl Density and Relaxations in Poly-(vinylbenzyltrimethylammonium)-b-poly(methylbutylene) Membranes for Electrochemical Applications. J. Am. Chem. Soc. 2018, 140, 1372–1384.
- (43) Agapov, A. L.; Sokolov, A. P. Decoupling Ionic Conductivity from Structural Relaxation: A Way to Solid Polymer Electrolytes? *Macromolecules* **2011**, *44*, 4410–4414.
- (44) Fan, J.; Willdorf-Cohen, S.; Schibli, E. M.; Paula, Z.; Li, W.; Skalski, T. J. G.; Sergeenko, A. T.; Hohenadel, A.; Frisken, B. J.; Magliocca, E.; Mustain, W. E.; Diesendruck, C. E.; Dekel, D. R.; Holdcroft, S. Poly(bis-arylimidazoliums) Possessing High Hydroxide Ion Exchange Capacity and High Alkaline Stability. *Nat. Commun.* 2019, 10, 2306.
- (45) Treichel, M.; Gaitor, J. C.; Birch, C.; Vinskus, J. L.; Noonan, K. J. T. Anion-Exchange Membranes Derived from Main Group and Metal-Based Cations. *Polymer* **2022**, *249*, No. 124811.

- (46) Landini, D.; Maia, A.; Rampoldi, A. Stability of Quaternary Onium Salts under Phase-Transfer Conditions in the Presence of Aqueous Alkaline-Solutions. *J. Org. Chem.* **1986**, *51*, 3187–3191.
- (47) Wu, S. K.; Lucki, J.; Rabek, J. F.; Rånby, B. Photo-Oxidative Degradation of Polynorbornene (Part I). *Polym. Photochem.* **1982**, 2, 73–85.
- (48) Lee, L.-B. W.; Register, R. A. Hydrogenated Ring-Opened Polynorbornene: A Highly Crystalline Atactic Polymer. *Macromolecules* **2005**, *38*, 1216–1222.
- (49) Selhorst, R.; Gaitor, J.; Lee, M.; Markovich, D.; Yu, Y.; Treichel, M.; Olavarria Gallegos, C.; Kowalewski, T.; Kourkoutis, L. F.; Hayward, R. C.; Noonan, K. J. T. Multiblock Copolymer Anion-Exchange Membranes Derived from Vinyl Addition Polynorbornenes. *ACS Appl. Energy Mater.* **2021**, *4*, 10273–10279.
- (50) Sanford, M. S.; Love, J. A.; Grubbs, R. H. A Versatile Precursor for the Synthesis of New Ruthenium Olefin Metathesis Catalysts. *Organometallics* **2001**, 20, 5314–5318.
- (51) Hong, M.; Cui, L.; Liu, S.; Li, Y. Synthesis of Novel Cyclic Olefin Copolymer (COC) with High Performance via Effective Copolymerization of Ethylene with Bulky Cyclic Olefin. *Macromolecules* **2012**, *45*, 5397–5402.
- (52) Paddon-Row, M. N.; Hartcher, R. Orbital Interactions. 7. The Birch Reduction as a Tool for Exploring Orbital Interactions Through Bonds. Through-Four-, -Five-, and -Six-Bond Interactions. *J. Am. Chem. Soc.* **1980**, *102*, *671*–*678*.
- (53) Sasaki, T.; Kanematsu, K.; Ando, I.; Yamashita, O. Molecular Design by Cycloaddition Reactions. 30. Photochemical Cycloadditions of Quadricyclane to Aromatic Hydrocarbons and o-Quinones. First Example of Photochemical Pericyclic $[4\pi + 2\sigma + 2\sigma]$ Addition. *J. Am. Chem. Soc.* **1977**, *99*, 871–877.

□ Recommended by ACS

Naturally Derived Allylated Gallic Acid for Interfacially Polymerized Membranes

Banan Alhazmi, Suzana P. Nunes, et al.

AUGUST 23, 2022

ACS SUSTAINABLE CHEMISTRY & ENGINEERING

READ 🗹

Dual-Cation Interpenetrating Polymer Network Anion Exchange Membrane for Fuel Cells and Water Electrolyzers

Lingping Zeng, Zidong Wei, et al.

MAY 24, 2022

MACROMOLECULES

READ 🗹

SEBS-Based Anion Exchange Membrane Grafted with N-Spirocyclic Quaternary Ammonium Cations for Fuel Cells

Jing Sang, Hong Zhu, et al.

SEPTEMBER 27, 2022

ACS APPLIED ENERGY MATERIALS

READ 🗹

Effects of Polyamide Chemistry on Solution Permeance in Molecular Layer-By-Layer Desalination Membranes

William D. Mulhearn and Christopher M. Stafford

APRIL 01, 2022

ACS APPLIED POLYMER MATERIALS

READ 🗹

Get More Suggestions >